Elastic anisotropic behaviour related to crack distributions in two gneisses

IOP Conf. Series: Earth and Environmental Science **833** (2021) 012005 doi:10.1088/1755-1315/833/1/012005

Elastic anisotropic behaviour related to crack distributions in two gneisses

T Rotonda

Department of Structural and Geotechnical Engineering, Sapienza Università di Roma, Rome, Italy

tatiana.rotonda@uniroma1.it

Abstract. Stress-strain response of foliated rocks shows that mechanical behaviour and degree of anisotropy are influenced by the spatial arrangement of phyllosilicates. But the anisotropy of these rocks is essentially due to the characteristics and distribution of cracks aligned with mica beds. At the laboratory scale, the elastic symmetry can be represented by the transverse isotropy, with the lowest elastic modulus perpendicular to the plane of aligned microcracks. These issues are discussed with reference to experimental data obtained for two gneisses of the same geological formation. The gneisses show a quite similar strength behaviour, but very different deformabilities. The measures of dynamic and static deformabilities under loading prove the influence of the progressive closure of open cracks on the compliance tensors of both gneisses. The relationship between the elastic parameters and the characteristics of the crack distributions is discussed in the framework of non-interacting crack models. Assuming the presence of two different sets of cracks, crack densities have been estimated. The different deformabilities of the two gneisses can be ascribed to their different microcrack distributions. The degree of anisotropy due to cracks reduces as stresses increase, differently for the two gneisses.

1. Introduction

Many rocks and rock masses exhibit anisotropic behaviour of deformability and strength, which often has to be taken into account to realistically predict the performance of engineering works.

Methods for estimating the state of stress by means of stress release measurements on tunnel walls or boreholes are very common. If deformability of the rock mass is anisotropic, measurements can be interpreted adopting the suitable anisotropic elastic model [1].

If deformability in anisotropic rock masses is investigated through plate-loading tests, more exhaustive results are provided if the measures are carried out in oriented boreholes, parallel and perpendicular to the principal deformability axis. In this case the proper elastic model accounts for anisotropy [30].

These examples prove that where the rock mass is anisotropic it determines a geotechnical complexity. Furthermore, investigations for geotechnical characterization of anisotropic rock masses often provide complex outcomes and discrepancies between the results of in situ and laboratory tests.

In order to reduce complexity, e.g. scale effects or inhomogeneity that can further affect engineering problems, studying the mechanical behaviour of anisotropic rocks at the laboratory scale is significant. Furthermore, experimental deformabilities of anisotropic rocks are relevant in the field of medium and low stresses, which are significant in practical applications.

In this paper the experimental data obtained in laboratory on two gneisses from the same geological formation are discussed in order to individuate their anisotropic elastic characteristics, described by the elasticity tensor. The laboratory tests included P- and S-wave velocity measurements; in the hypothesis of the transverse isotropy symmetry, properly oriented measurements allowed the estimate of the dynamic elasticity tensor. The closure of cracks was investigated by means of isotropic triaxial tests. Furthermore, static deformabilities measured under deviatoric stress on specimens with different angle of schistosity allowed the estimate of the static compliance tensor. From static and dynamic measurements, crack density distributions of open cracks were estimated for both the gneisses, evidencing their differences.

2. Anisotropy in foliated rocks

The observed anisotropic behaviour of intact rocks is caused by a preferred orientation of one or more of the following structural elements:

(i) the crystal lattices of the rock-forming minerals;
(ii) non-equidimensional grains or crystal (taking only their shape into account);
(iii) non-equidimensional voids, particularly open or closed microcracks.

In most cases a close connection is observed between the orientation of the three types of structural elements. Accordingly, even if the second type is immediately apparent, it is not essential, as anisotropy depends on the other two types. A typical example is the case of the foliated rocks.

Foliated rocks are characterized by the presence of planar structures, produced by the stresses applied during the pre-metamorphic stage (developing a primary stratification) and/or the metamorphic process (resulting in cleavage and schistosity). Often, the term foliation is restricted to planar structures formed by metamorphic processes, which are considered a secondary foliation.

The cleavage and schistosity planes are different in the scale, which is, respectively, the small scale (from mm to tens of mm) and the intermediate scale (hundreds of mm). The foliation is called schistosity in case of coarse-grained rocks (schists), whose fabric is characterized by closely spaced parallel beds (schistosity planes) along which the phyllosilicate minerals concentrate. Beds of phyllosilicates are separated by bands of other crystals (quartz, feldspar), more or less thick. This alternation is apparent in gneissic rocks, where the metamorphic process produced levels with different mineralogical composition. Gneiss texture is characterized by large crystals and schistosity planes are often sharply undulated, surrounding lenses of porphyroblasts of quartz or feldspar (augen-gneiss).

In foliated rocks the micas always show a preferred planar orientation, whilst the other minerals are often not markedly oriented. It is often reasonable to assume for crystal lattices orientation, which is the "intrinsic" anisotropy, the transverse isotropy (TI) or the orthotropic symmetry.

Nevertheless, the intrinsic anisotropy has been proven to be of little relevance as the schistosity planes of schists and gneiss are planes of weakness, where, under applied stresses, microcracks could develop. In these rocks, the coincidence between the orientation of the crystal lattices and the associated microcracks lead to the prevalence of a planar structure, and the TI or the orthotropic symmetry can be assumed.

3. Elastic characteristics of anisotropic rocks

In the generalized Hooke's law, the elastic properties of an anisotropic medium are represented by a fourth-order elasticity tensor which relates the stress tensor to the strain tensor. According to the contracted notation, when engineering strains ε_r and stresses σ_q are used, the constitutive equations becomes:

$$\varepsilon_r = \mathbf{M}\,\sigma_q \qquad r,q = 1,6 \tag{3.1}$$

where the second-order tensor **M** (compliance matrix) and its inverse **L** (stiffness matrix) are two indexes matrixes.

Due to some energy restrictions, the elasticity tensor presents only 21 independent components; however, rocks often show elements of symmetry, hence reducing the number of the components. For

rocks characterized by orthotropic symmetry the non-null terms are 9, whereas for the transverse isotropy (TI) they are only 5. If not differently supposed, the next equations refer to TI symmetry.

Assuming the principal symmetry directions as the reference system 1, 2, 3 (Figure 1) the compliance matrix **M** of a transversal isotropic rock can be written in terms of the engineering elastic parameters:

$$\mathbf{M}=\begin{bmatrix} M_{11} & M_{12} & M_{13} & 0 & 0 & 0 \\ & M_{11} & M_{13} & 0 & 0 & 0 \\ & & M_{33} & 0 & 0 & 0 \\ & & & M_{55} & 0 & 0 \\ & \text{sym} & & & M_{55} & 0 \\ & & & & & M_{66} \end{bmatrix}=\begin{bmatrix} \frac{1}{E_1} & -\frac{\nu_{21}}{E_1} & -\frac{\nu_{31}}{E_3} & 0 & 0 & 0 \\ & \frac{1}{E_1} & -\frac{\nu_{31}}{E_3} & 0 & 0 & 0 \\ & & \frac{1}{E_3} & 0 & 0 & 0 \\ & & & \frac{1}{G_{31}} & 0 & 0 \\ & \text{sym} & & & \frac{1}{G_{31}} & 0 \\ & & & & & \frac{1}{G_{21}} \end{bmatrix} \tag{3.2}$$

If TI symmetry is assumed, axis 3 is oriented as the normal to the isotropic plane, axes 1 and 2 are equivalent, and the 5 independent elastic parameters could be: 2 Young's moduli, E_1 and E_3; 1 shear modulus, G_{13}; 2 Poisson's coefficients, ν_{31} and ν_{21}. In foliated rocks the polar axis 3 is in practice the direction corresponding to the minor principal modulus, as will be shown in the following.

A generic reference system will be indicated as 1*, 2*, 3* (Figure 1) and **M*** will be the corresponding compliance matrix. The transformation formulas containing the direction cosines of the new reference system 1*, 2*, 3* with respect to 1, 2, 3 are given by Lekhnintski [17]. The angle θ is defined as the angle between the normal to the isotropic plane 3 and the direction of axis 3* (Figure 1).

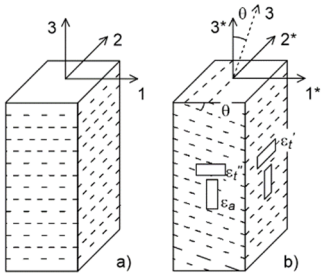

Figure 1. Orientation of the reference system in a rock with TI symmetry (left); generic reference system and definition of the θ angle (right).

3.1. Static deformability

Under uniaxial loading the longitudinal ε_a and radial strains ε_t' and ε_t'' measured in specimens whose loading axis σ_a forms an angle θ with respect to the axis of elastic symmetry (Figure 1, right) are related to the coefficients of deformability through the followings [1]:

$$\begin{bmatrix} \frac{\mathrm{d}\varepsilon_a}{\mathrm{d}\sigma_a} \\ \frac{\mathrm{d}\varepsilon_t'}{\mathrm{d}\sigma_a} \\ \frac{\mathrm{d}\varepsilon_t''}{\mathrm{d}\sigma_a} \end{bmatrix}=\begin{bmatrix} \frac{1}{E_\theta} \\ -\frac{\upsilon_\theta'}{E_\theta} \\ -\frac{\upsilon_\theta''}{E_\theta} \end{bmatrix}=\begin{bmatrix} \operatorname{sen}^4\theta & 0 & 2\frac{\operatorname{sen}^2 2\theta}{4} & \cos^4\theta & \frac{\operatorname{sen}^2 2\theta}{4} \\ 0 & \operatorname{sen}^2\theta & \cos^2\theta & 0 & 0 \\ \frac{\operatorname{sen}^2 2\theta}{4} & 0 & \operatorname{sen}^4\theta+\cos^4\theta & \frac{\operatorname{sen}^2 2\theta}{4} & -\frac{\operatorname{sen}^2 2\theta}{4} \end{bmatrix}\begin{bmatrix} M_{11} \\ M_{12} \\ M_{13} \\ M_{33} \\ M_{55} \end{bmatrix} \tag{3.3}$$

If the shear modulus G_{SV} is introduced as a function of the other moduli (Saint Venant hypothesis), the elastic constants are reduced at 4 [17][15]:

$$M_{44} = M_{11} + M_{33} - 2M_{13}$$
$$\frac{1}{G_{SV}} = \frac{1+\nu_{13}}{E_1} + \frac{1+\nu_{31}}{E_3} \tag{3.4}$$

This relationship imply that the shear modulus is invariant for a rotation within a plane passing through the principal axis, i.e. it is independent on the θ angle. The Saint-Venant hypothesis, also called isoG hypothesis, is often assumed in practical applications, since it simplifies many problems concerning anisotropic bodies.

The deformabilities measured under uniaxial loading (equation (3.3)) can be also written as a function of the engineering elastic moduli:

$$\begin{aligned}
\frac{\mathrm{d}\varepsilon_a}{\mathrm{d}\sigma_a} &= \frac{1}{E_\theta} = \frac{1}{2}\left(\frac{1}{E_3} + \frac{1}{E_1}\right) + \frac{1}{2}\left(\frac{1}{E_3} - \frac{1}{E_1}\right)\cos 2\theta + \left(\frac{1}{G_{13}} - \frac{1}{G_{SV}}\right)\mathrm{sen}^2\theta\cos^2\theta \\
\frac{\mathrm{d}\varepsilon_t'}{\mathrm{d}\sigma_a} &= -\frac{\upsilon_\theta'}{E_\theta} = -\frac{\upsilon_{31}}{E_3} - \left(\frac{\upsilon_{12}}{E_1} - \frac{\upsilon_{31}}{E_3}\right)\sin^2\theta \\
\frac{\mathrm{d}\varepsilon_t''}{\mathrm{d}\sigma_a} &= -\frac{\upsilon_\vartheta''}{E_\theta} = -\frac{\upsilon_{31}}{E_3} - \left(\frac{1}{G_{13}} - \frac{1}{G_{SV}}\right)\mathrm{sen}^2\theta\cos^2\theta
\end{aligned} \tag{3.5}$$

3.2. Dynamic deformability

In case dynamic measurements are performed, the equation of motion, excluding any body forces, for a plane wave in a continuum body ([2], [12]) have to be introduced. In homogeneous media we define locally the phase velocity as the velocity of advance of the wavefront, and the phase angle θ as the angle between the wavefront normal and the direction of the energy propagation. The phase velocities are related to the elastic stiffness tensor (Christoffel tensor) through the vector of the particle oscillation and density ρ of the rock.

The phase velocities are the P-wave and two shear waves, SR- (vibration direction contained in the polar isotropic plane) and SP-wave (vibration direction perpendicular to the SR-wave). Assuming that the variations in velocity could be considered as those of a TI symmetry, where the axis 3 is the axis of circular symmetry, measurements of V_{SR} and V_{SP} velocities on cylindrical specimens with axis along the direction 1 correspond to velocities V_{12} and V_{13}.

Assuming the phase angle θ with respect to the polar axis, the solution of Christoffel's equations leads to the following relations between velocities and the stiffness tensor $\mathbf{L} = \mathbf{M}^{-1}$:

$$\begin{aligned}
\rho V_P^2 / \rho V_{SP}^2 &= 0.5\left[L_{33} + L_{44} + (L_{11} - L_{33})\sin^2\theta \pm D(\theta)\right] \\
\rho V_{SR}^2 &= 0.5\,(L_{66} + L_{44}) - (L_{66} - L_{44})\cos^2\theta
\end{aligned} \tag{3.6}$$

where the term $D(\theta)$ is defined by:

$$\begin{aligned}
D(\theta) = (L_{33} - L_{44})^2 + 2\Big[2(L_{13} + L_{44})^2 - (L_{33} - L_{44})(L_{11} + L_{33} - 2L_{44})\Big]\sin^2\theta + \\
+\Big[(L_{11} + L_{33} - 2L_{44})^2 - 4(L_{13} + L_{44})^2\Big]\sin^4\theta
\end{aligned} \tag{3.7}$$

The components of the stiffness tensor can be determined from the velocities, as the terms L_{11}, L_{33}, L_{55} and L_{66} derive directly from the P- and S-wave velocities measured along the principal directions

(e.g. $L_{11} = \rho V_1^2$). For determining the term L_{13} measures of the P- and SP-wave velocities on specimens with a θ angle different from 0 ° and 90 ° are required, for example using the equation:

$$D(\theta) = \rho\left(V_P^2(\theta) - V_{SP}^2(\theta)\right) \tag{3.8}$$

4. Modelling elastic deformability of microcracks

The effect of open and closed cracks in rock deformation and the influence of progressive closing of microfissures results in the non-linear stress-strain behaviour. The relevance of microcracks in governing the anisotropic deformability is asserted by the strong dependence of the degree of anisotropy on the applied stress. Moreover, the variation of elastic constants with the orientation of the specimen is quite different from that predicted by the intrinsic compliance tensor of elasticity of the matrix.

In a homogeneous microfissured medium, having a very low porosity, the anisotropy is the result of the preferred orientation of its constituent minerals (par. 2): minerals ('intrinsic' or 'solid matrix' anisotropy) and microcracks. The ultimate symmetry is due to the superimposition of the various elements of symmetry, and generally, it results of a lower order.

The elastic tensor of deformability (compliance tensor) can be considered as the sum of two contributions, deriving respectively from the solid matrix $\mathbf{M}_m$ and from the voids $\Delta\mathbf{M}$:

$$\mathbf{M} = \mathbf{M}_m + \Delta\mathbf{M} \tag{4.1}$$

The matrix of deformability $\mathbf{M}_m$ can be determined by averaging the deformabilities of the different minerals, referred to a unique reference system, taking into account the distribution of their orientation and their relative volume [13].

For many types of crystalline rocks, including foliated rocks, the deviation from isotropy of the intrinsic elastic tensor is relatively modest [5]. In case the isotropic model is assumed, the averaged parameters E_m and ν_m can be thus evaluated:

$$\begin{aligned} E_m &= 3*(M_{11}^m + M_{22}^m + M_{33}^m)^{-1} \\ \nu_m &= -\frac{E_m}{3}(M_{12}^m + M_{23}^m + M_{13}^m) \end{aligned} \tag{4.2}$$

Void contribution to rock compliance $\Delta\mathbf{M}$ can be evaluated on the basis of different models. The simplest theoretical schemes that have been proposed in the literature derive from two different approaches: i) 'equivalent stress' models, which lead to the so-called non-interacting crack models [22], [18]; ii) 'equivalent material' models, such as the self-consistent model [23], or the differential self-consistent model [21], [6].

In the non-interacting crack models, each crack is considered as being isolated and its effects on the state of stress are not influenced by the presence of other cracks; this leads to higher elastic moduli with respect to the other models. Numerical simulations [19] have shown that if cracks are randomly distributed, interaction does not occur also for high crack densities. As the contribution of any crack distribution can be obtained by a simple superimposition of the effects of each crack, these models lead to great simplifications in the analytical expressions. In the following, the hypothesis of non-interacting cracks will be adopted.

4.1. Model based on the normal and tangential stiffnesses

In the equivalent continuous medium models, typical of the rock mass scale, the effect of discontinuities is often taken into account in a global and homogenized way. The equivalent medium is weaker and less stiff than the intact rock. An essential condition for the use of such models is that the mean spacing of the various sets of discontinuities is small compared to the characteristic dimensions of the volume of interest (REV).

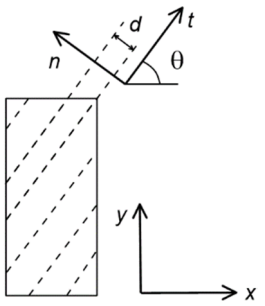

Figure 2. Orientation of the local reference system of a single set of cracks and definition of spacing d and angle of orientation θ.

This model can be extended to the small scale by associating a set of discontinuities to a set of microcracks. In the following, a classical procedure is illustrated to obtain the equivalent elasticity matrix for a volume containing one or more sets of cracks [10]. The contribution of microcracks to rock compliance $\Delta\mathbf{M}$ can be evaluated on the basis of deformability, orientation and frequency of each set.

The development of plastic deformations, i.e. fracture of microcracks, is not treated, thus limiting the application of the model to the case of microcracks causing normal and shear deformations in elastic conditions.

In the elementary volume represented in Figure 2 there is only one set of continuous microcracks with constant spacing d; its orientation is identified by the angle θ between the global x, y reference system and the local n, t reference system. The set is represented by linear elements in a 2D continuum, or by planar elements in a 3D continuum, being continuous (without rock bridges) and of negligible volume.

Under these hypotheses, the analysis is simplified because the intact material and the set of cracks are subject to the same state of stress. The problem is treated under plane deformation conditions ($\varepsilon_z = 0$), assuming that the third z axis is common to the local and global reference systems.

If the intact rock is considered isotropic with deformability matrix $\mathbf{M}_\mathrm{m}$, it is not necessary to introduce a reference system for the rock.

The behaviour of a single set of cracks in elastic conditions is described by means of the stiffness constants K_n, K_s associated respectively to the relative displacement in the normal and tangential direction [10]. To determine the contribution of the cracks to the global deformation of the elementary volume, the relative displacements are divided by the mean spacing d.

Thus, the equivalent deformability due to the set of cracks is described by the matrix $\Delta\mathbf{M}_\mathrm{c}^{\mathrm{n,t}}$, where the subscript 'c' is related to the set of cracks, in the local reference system:

$$\Delta\mathbf{M}_\mathrm{c}^{\mathrm{n,t}} = \begin{bmatrix} \dfrac{1}{K_\mathrm{n}\, d} & 0 \\ 0 & \dfrac{1}{K_\mathrm{s}\, d} \end{bmatrix} \tag{4.3}$$

In the case of continuous cracks, the stress on their plane must be in equilibrium with the external stress. The equivalent terms of deformation $\Delta\mathbf{M}_\mathrm{c}$ due to the single set in the global reference system are provided by the transformation matrix $\mathbf{C}_\mathrm{c}$ containing the direction cosines of the new reference system:

$$\Delta\mathbf{M}_\mathrm{c} = \mathbf{C}_\mathrm{c}{}^{\mathrm{T}}\, \Delta\mathbf{M}_\mathrm{c}^{\mathrm{n,t}}\, \mathbf{C}_\mathrm{c}; \qquad \mathbf{C}_\mathrm{c} = \begin{bmatrix} s^2 & c^2 & -2cs & 0 \\ -cs & cs & c^2 - s^2 & 0 \end{bmatrix} \quad \begin{matrix} c = \cos\theta \\ s = \sin\theta \end{matrix} \tag{4.4}$$

To obtain the overall deformation of the elementary volume, it is sufficient to apply the equation (4.1), adding the two deformabilities.

In case of j-sets of cracks, each of them differently oriented and spaced, through the θ_j angle and the spacing d_j, respectively, local $\Delta\mathbf{M}_{\mathrm{c}\,j}^{\mathrm{n,t}}$ and then global $\Delta\mathbf{M}_{\mathrm{c}\,j}$ deformability matrixes can be introduced.

The overall deformation of the equivalent cracked medium is given summing the contribution of the intact rock to the equivalent contributions of the various sets of cracks:

$$\mathbf{M} = \mathbf{M}_{\mathrm{m}} + \sum_j \Delta\mathbf{M}_{\mathrm{c}\,j} \tag{4.5}$$

In case of non-continuous cracks, the analysis has to take into account that the stress conditions acting on the sets of cracks are no longer independent on each other.

4.2. Model based on the crack density tensor

In the hypothesis of non-interacting cracks, each set of cracks gives its contribution as being isolated.

Assuming that the anisotropy of the solid matrix is negligible, the contribution of the voids to the compliance matrix $\Delta\mathbf{M}$ can be considered as the sum of two terms:

$$\Delta\mathbf{M} = \Delta\mathbf{M}^{\mathrm{A}}(\mathbf{F}_{ij}) + \Delta\mathbf{M}^{\mathrm{B}}(\mathbf{F}_{ijkl}) \tag{4.6}$$

where the matrixes $\Delta\mathbf{M}^{\mathrm{A}}$ and $\Delta\mathbf{M}^{\mathrm{B}}$ depend, other than on the matrix deformability $\mathbf{M}_{\mathrm{m}}$, on the second- and fourth-order tensors F_{ij} and F_{ijkl}, respectively. For penny-shaped cracks having diameter 2 a and orientation of the normal, **n**, the so-called crack density tensors **F** ([18] [19] [25]) are defined by the followings:

$$\begin{aligned} F_{ij} &= \frac{1}{V}\sum\left(a^3 n_i n_j\right) \\ F_{ijkl} &= \frac{1}{V}\sum\left(a^3 n_i n_j n_k n_l\right) \end{aligned} \tag{4.7}$$

where V is the involved volume.

If intrinsic anisotropy is neglected, the matrix $\Delta\mathbf{M}$ depends on the tensor $\mathbf{M}_{\mathrm{m}}$ through the term Q_{m}, i.e. on the Young's modulus and Poisson's coefficient E_{m} and ν_{m} (equation (4.2)), thus defined:

$$Q_{\mathrm{m}} = \frac{16}{3}\frac{(1-\nu_{\mathrm{m}}^2)}{E_{\mathrm{m}}} \tag{4.8}$$

For a single open crack, having its normal directed along axis 3, the non-null components of the compliance matrix $\Delta\mathbf{M}$**,** are [15]:

$$\begin{aligned} \Delta M^{\mathrm{A}}_{3333} &= 4\,\Delta M^{\mathrm{A}}_{1313} = 4\,\Delta M^{\mathrm{A}}_{2323} = \frac{Q_{\mathrm{m}}}{1-0.5\nu_{\mathrm{m}}}\frac{a^3}{V} \\ \Delta M^{\mathrm{B}}_{3333} &= -0.5\nu_{\mathrm{m}}\,\frac{Q_{\mathrm{m}}}{1-0.5\nu_{\mathrm{m}}}\frac{a^3}{V} \end{aligned} \tag{4.9}$$

By referring the contribution of each cracks to the same reference system, the overall contribution is given by

$$\begin{aligned} \Delta M^{\mathrm{A}}_{ijkl} &= \frac{Q_{\mathrm{m}}}{1-0.5\nu_{\mathrm{m}}}\frac{1}{4}\left(\delta_{ik}F_{jl} + \delta_{il}F_{jk} + \delta_{jk}F_{il} + \delta_{jl}F_{ik}\right) \\ \Delta M^{\mathrm{B}}_{ijkl} &= -0.5\nu_{\mathrm{m}}\frac{Q_{\mathrm{m}}}{1-0.5\nu_{\mathrm{m}}}F_{ijkl} \end{aligned} \tag{4.10}$$

where δ_{ij} is the Kronecker delta function.

It can be recognized that tensor $\Delta\mathbf{M}^{\mathrm{A}}$ shows an orthotropic symmetry, having its principal planes and axes corresponding to those of tensor F_{ij}. By adopting the two-subscripts notation, tensor $\Delta\mathbf{M}^{\mathrm{A}}$, referred

to its principal axes, is given by:

$$\Delta\mathbf{M}^{\mathrm{A}} = \frac{Q_{\mathrm{m}}}{1-0.5\nu_{\mathrm{m}}}\begin{bmatrix} F_{11} & 0 & 0 & 0 & 0 & 0 \\ & F_{22} & 0 & 0 & 0 & 0 \\ & & F_{33} & 0 & 0 & 0 \\ & & & F_{22}+F_{33} & 0 & 0 \\ & sym & & & F_{11}+F_{33} & 0 \\ & & & & & F_{11}+F_{22} \end{bmatrix} \tag{4.11}$$

Tensor $\Delta\mathbf{M}^{\mathrm{B}}$ introduces non orthotropic additional terms. As their terms are sensibly lower with respect to those of $\Delta\mathbf{M}^{\mathrm{A}}$ (due to the multiplier $0.5\nu_{\mathrm{m}}$ in equation (4.10)), their contribution could be possibly considered negligible.

With the aim of estimating the effect of cracks from the velocity measurements applying the equations (3.6), several authors ([16] [31]) have studied the direct relationship between the stiffness tensor **L** and the crack density tensor. These approaches give reliable results only for low values of the density, while introducing the effect of cracks through the compliance matrix **M** does not have this restriction.

As the measurement of S-wave velocities on heavily microcracked rocks at low confinement stresses are often difficult and affected by uncertainties, the model can be simplified using the P-wave velocities in the principal directions only. A reduced matrix **M**, which represents a portion (3 x 3) of the compliance terms of an orthotropic microcracked rock, can be introduced:

$$\mathbf{M} = \begin{bmatrix} {M_{11}}^{\mathrm{m}} + \Delta M_{11} & {M_{12}}^{\mathrm{m}} & {M_{13}}^{\mathrm{m}} \\ & {M_{22}}^{\mathrm{m}} + \Delta M_{22} & {M_{23}}^{\mathrm{m}} \\ sym & & {M_{33}}^{\mathrm{m}} + \Delta M_{33} \end{bmatrix} \tag{4.12}$$

From the P-wave velocities in the principal directions (equation (3.6)), the principal stiffness moduli L_{11}, L_{22} and L_{33} can be directly determined and then the related compliance moduli. Once the moduli of the solid rock are assigned, the crack-induced compliance terms ΔM_{11}, ΔM_{22} and ΔM_{33} can be estimated by means of an iterative procedure applied to equations (4.1) and (4.12).

From equations (4.11) and (4.12) the crack-induced compliance ΔM_{11} is related to the corresponding principal terms of the crack density tensors by the following relationship:

$$\Delta M_{11} = \Delta M_{11}^{\mathrm{A}} + \Delta M_{11}^{\mathrm{B}} = \frac{Q_m}{1-0.5\nu_m}\left(F_{11} - \frac{\nu_m}{2} F_{1111}\right) \tag{4.13}$$

and the terms for the other principal directions are simply obtained by permutation of the subscripts. The values of F_{ii} can be easily obtained if the components F_{iiii} are neglected; alternatively, they can be linearly related to the terms F_{ii}, when a given type of crack distribution is assumed.

Total crack density e_{T} is thus defined by:

$$\begin{aligned} e_{\mathrm{T}} &= \sum\frac{a^3}{V} = F_{11}+F_{22}+F_{33} = \\ &= \frac{1-0.5\nu_m}{Q_m}\left(\Delta M_{11}+\Delta M_{22}+\Delta M_{33}\right) + \frac{\nu_m}{2}\left(F_{1111}+F_{2222}+F_{3333}\right) \end{aligned} \tag{4.14}$$

If the effect of intrinsic anisotropy and of the compliance $\Delta\mathbf{M}^{\mathrm{B}}$ are neglected, the compliance tensor **M** (equation (4.12)) can be simplified. It can be stated without introducing significant errors that in this case any distribution of cracks produces an orthotropic symmetry, where the principal axes coincide

with those of the F_{ij} tensor. In practice, with regard to the elastic properties of the rock, any distribution of cracks is equivalent to three mutually orthogonal sets of cracks.

In these simplified hypotheses, equations (4.11) and (4.12) show that the shear moduli of the microcracked rock are not independent from the other two elastic moduli of the isotropic matrix (i.e. the isoG hypothesis is valid and the transversal deformations do not depend on cracks). If anisotropy derives only from the density and orientation of microcracks, the independent elastic parameters are 4 (instead of the 9 parameters of a general orthotropic medium): i.e., 3 principal Young's moduli and 1 coefficient of transversal deformation, deriving from the intrinsic moduli $M_{12} = M_{13} = M_{23} = -\nu_m/E_m$ (equation (4.2)).

5. Experimental observation of anisotropy in foliated rocks

The elastic characteristics are often investigated through dynamic measurements, i.e., velocity of ultrasonic waves, which require the mathematical inversion technique to determine the elastic moduli [31]. Experimental tests for the individuation of the elastic symmetry of anisotropic rocks include measurements on spherical specimens, specimens having polyhedric faces or sets of cylindrical specimens, cored at different orientations from the same block ([14] [27] [7]).

The experimental results obtained by Birch [4] indicated that the increase in the P-wave velocity under loading is due to closure of the microcracks. Measurement of the P-wave velocity is very effective for evaluating the possible microcracks oriented according to preferential directions, such as to contribute significantly to anisotropic properties [25]. At high stresses, the anisotropy of the P- and S-waves is caused solely by the alignment of the minerals ([4] [27]).

The effect of stress on rock anisotropy has been observed by many Authors also through measurements of static deformability under deviatoric loads ([9]). Regression statistical analyses applied at measurements from oriented specimens to obtain the global stiffness matrix **L** (equations (3.6) and (3.7)) and the global compliance matrix **M** (equations (3.3)) are commonly used ([14] [3] [11] [20] [7]).

The main characteristics of the degree of anisotropy can be expressed by the ratios R_V and R_E. The ratio R_G can also give some insights into the observed behaviour. These ratios are defined by the following relations:

$$R_V = \left(\frac{V_1}{V_3}\right)^2; \qquad R_E = \frac{E_1}{E_3}; \qquad R_G = \frac{G_{SV}}{G_{13}} \tag{5.1}$$

The anisotropy ratio R_V is based upon P-wave velocities, where axis 3 is perpendicular to the main planar structure of the rock, and axis 1 is directed along a possible lineation (in case of orthotropic symmetry).

The isoG hypothesis is satisfied when the ratio R_G is equal to 1.

The compliance matrix $\mathbf{M}_m$ of foliated rocks consisting of alternating layers of perfectly oriented mica beds and of randomly oriented quartz crystals could be determined by averaging techniques [13]. The mica content of typical gneisses is 10 - 20%, while for schists it may be as much as 50 % or more; the resulting intrinsic anisotropy ratio R_E varies from 1.1 to 2.0, for gneisses and schistose rocks, respectively.

Experimental data of R_V and R_E ratios on foliated rocks strongly differ from the values of the matrix, indicating that these ratios are influenced by the state of stress. In order to compare the ratios among different rocks they should be firstly referred to the same loading path and stress level, but this do not ensure a valid comparison as rocks have different crack distributions. For the same rock the trend of the ratios under stress levels are related to the evolution of microcracks [11].

6. Mechanical behaviour of the investigated rocks

An extensive campaign of laboratory tests on a foliated metamorphic rock (Antigorio gneiss) was carried out. Rock was sampled in a zone where an underground hydroelectric power station was planned, in proximity of the Toce river valley (Central Alps, Italy).

From an exploratory tunnel at a depth of about 700 m, boreholes were drilled to retrieve samples for rock characterization. With the aim of studying the mechanical effects of stress relief on the deformability of the crystalline rock, a very large block (2.7 × 0.76 × 1.06 m) was detached from a quarry located on a side of the Toce river.

Hereinafter, the samples coming from the tunnel and quarry will be referred to, respectively, as 'deep gneiss' (D-gneiss) and 'superficial gneiss' (S-gneiss).

Cores of various diameters providing specimens for mechanical characterization and for studying anisotropy were taken. Samples in the shape of sphere (147 mm in diameter), hexadecagon (straight prisms with sixteen flat lateral surfaces, distant at about 140 mm) and cylinder (147 mm in diameter) were prepared.

To describe the mechanical behaviour of the two rocks various tests were carried out on NX specimens (54 mm in diameter, height-to-diameter ratio equal to 2). Uniaxial (UN) and isotropic compression (ID and IDE) tests were performed. In ID and IDE tests isotropic pressure up to 60 MPa was applied. During the tests, the longitudinal and shear velocities in the direction of the loading axis (ID tests), the axial and circumferential strains (IDE tests), and finally both the velocities and the strains (UN tests) were measured.

6.1. Mineralogical properties

The mineralogical composition of the two gneisses, obtained from modal analyses on thin sections observed at the polarized light microscope, was very similar for D- and S-gneiss: quartz 40-39 %, K-feldspar 23 %, biotite 15-13 %, plagioclase 22-25 %.

Schistosity is in the form of thin wavy layers of biotite which surround the other crystals, slightly elongated along the schistosity, giving the rock a 'nodular' fabric. Upon microscopic examination (Figure 3) the S-gneiss shows coarser grain and thicker mica beds than D-gneiss, which has finer grains and thinner and more frequent mica beds. In the D-gneiss the mica beds have greater continuity.

The observation of the thin sections (Figure 3) has also revealed that the schistosity planes are not perfectly planar but arranged along weakly inclined alignments whose intersection gives rise to a rhomboid texture. The cross-planes form acute angles of ± 8° and ± 12° in D- and S-gneiss, respectively.

Moreover, the biotite, whose cleavage planes are oriented as the lattices, appears affected by very long and frequent parallel microcracks in the S-gneiss, while the microcracks are shorter and less frequent in the D-gneiss. The other minerals show microcracks without a preferential orientation. In both gneisses, cracks of crystal boundaries can generally be considered with matching lips.

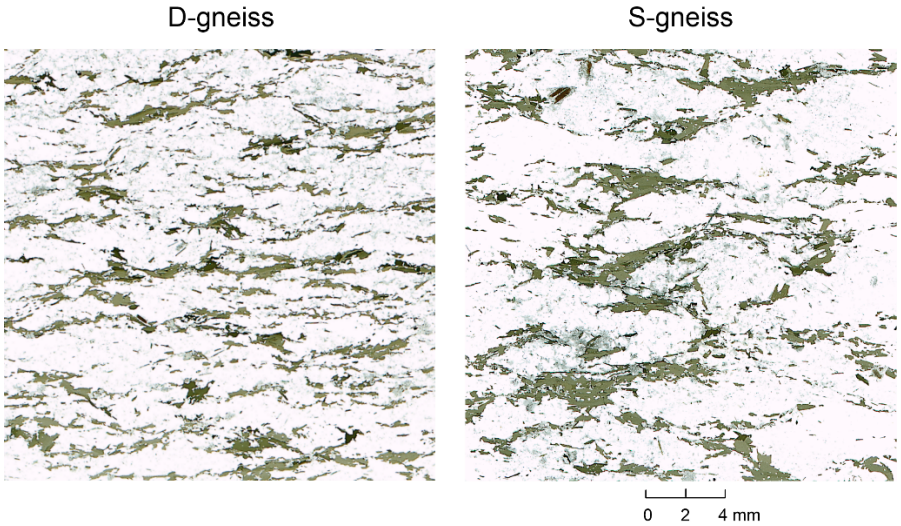

Figure 3. Thin sections of the two gneisses (green colour is associated to biotite crystals).

A quantitative count of the lengths of microcracks on single crystals (biotite and quartz) in thin petrographic sections were carried out. In the hypothesis that microcracks were continuous, the length l of microcracks over the investigated areas (Table 1) provided crack frequency and related mean spacing d.

Table 1. Mean values of crack frequency measured in crystals of biotite and quartz.

	D-gneiss	S-gneiss
$\Sigma l/Area$ biotite (mm^{-1})	0.471	0.663
$\Sigma l/Area$ quartz (mm^{-1})	0.332	0.722

6.2. Physical properties

For the mechanical characterization 17 and 50 cylindrical NX specimens of the D-gneiss and S-gneiss were prepared, respectively. In order to determine dry density ρ_d geometrically regular specimens were dried up to a constant weight under vacuum or in an oven at very mild temperatures, in order to avoid thermal microfissuring.

Solid matrix density ρ_s has been determined with a helium picnometer on finely grounded materials. From densities of the solid matrix and of the dry specimens the mean value of the total porosity ϕ has been estimated, resulting slightly higher in S-gneiss. These physical properties are reported in Table 2.

Table 2. Mean values of density, solid matrix density and porosity.

	D-gneiss	S-gneiss
ρ (Mg/m^3)	2.714	2.683
ρ_s (Mg/m^3)	2.754	2.744
ϕ (%)	1.46	1.91

6.3. Dynamic properties in unstressed conditions

Ultrasonic velocities of P- and S-waves have been determined by measuring the transit time of a square wave, through Panametrics piezoelectric transducers (15 mm in diameter, 1 MHz in frequency).

Measurements of P-wave velocity on spherical, cylindrical and hexadecagonal samples have indicated that the gneisses are characterized by an orthotropic symmetry, with three planes of symmetry, one of which coincides with the schistosity plane.

The range of variation of P-wave velocities measured in the two gneisses is reported in Table 3, where the $V_{1\text{-}2}$ velocity refers to the measurements in the schistosity plane without distinction between the maximum and intermediate value. In Table 3 also two anisotropy ratios are reported: R_V (equation (5.1)), relative to the maximum and minimum moduli, and $(V_1/V_2)^2$, relative to the maximum and intermediate modules (in the plane of schistosity).

Table 3. Range of P-wave velocities and dynamic anisotropy ratios.

	D-gneiss	S-gneiss
$V_{1\text{-}2}$ (km/s)	4.2-5.0	3.0-3.8
V_3 (km/s)	3.6-4.6	1.8-2.9
$(V_{1\text{-}2}/V_3)^2$ (-)	1.4	2.6
$(V_1/V_2)^2$ (-)	1.2	1.2

As expected, the polar axis 3 is the direction corresponding to the minor principal velocity. The principal velocities of S-gneiss are on average lower with respect to D-gneiss, providing a higher anisotropy ratio. The anisotropy ratio in the polar plane is instead almost the same and quite low for the two rocks, thus assessing that assuming a TI symmetry does not result in a severe approximation.

Velocities of P- and S-waves were also measured on all the specimens (NX geometry) prepared for the tests under loading. As the orthotropic symmetry, the velocity measurements of P-waves measured in the schistosity plane on these specimens are to be considered between the maximum and the intermediate value. Figure 4 shows the P-wave velocity measurements for differently oriented specimens, and also the elastic model of equation (3.6), derived from a regression analysis on the measurements.

6.4. Strength properties

To investigate the mechanical behaviour of the gneisses, uniaxial (UN) tests on NX cylindrical specimens were performed. 5 and 13 specimens, with different orientation of the schistosity planes, were tested for D- and S-gneiss, respectively.

The macroscopic failure surfaces observed in specimens subjected to deviatoric loading cross the matrix in specimens whose θ angle equals 0 ° and 90 °, while they develop along the schistosity plane in the specimens with $\theta = 45$ ° and are of mixed type in specimens with the remaining angles.

The measured strengths (Figure 5, Table 4) show that their maximum values are experienced at $\theta = 0$ ° for both gneisses. For θ angle close to the minimum strength, few specimens were tested. The resulted degrees of anisotropy were 2.1 and 1.5 for D- and S-gneiss, respectively, consistently with those proposed by Ramamurthy [26] for gneiss.

Table 4. Mean values of the minimum and maximum uniaxial compressive strengths, revealed at different schistosity angles.

	D-gneiss	S-gneiss
UCS_{max} (MPa)	124.1	119.9
UCS_{min} (MPa)	58.9	78.6

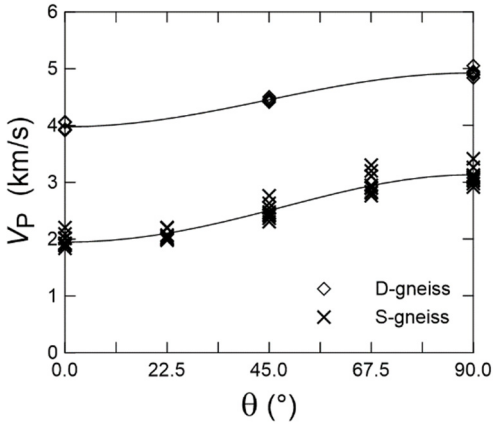

Figure 4. P-wave velocity measurements (symbols) on variously oriented NX specimens of D- and S-gneiss. Elastic model applied to the experimental data is represented by continuous lines.

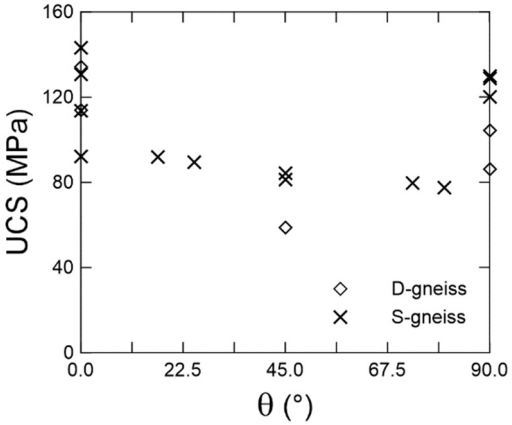

Figure 5. Uniaxial strength on specimens of D- and S- gneiss.

6.5. Dynamic measurements under loading

Under compression loading tests (ID and UN) velocities were measured through piezoelectric transducers (nominal frequency of 1 MHz) enclosed in the load platens. Three velocities along the loading axis were measured: the longitudinal wave and two shear waves: SR- (vibration direction in the schistosity plane) and SP-wave (vibration direction perpendicular to the SR-wave) (par. 3.2).

Isotropic compression tests (ID) were carried out, using the conventional Hoek cell, up to the maximum confinement stress of 60 MPa. 7 and 10 specimens, with different orientation of the schistosity planes, were tested for D- and S-gneiss, respectively.

Some of the same specimens were driven to failure under uniaxial conditions (UN tests), after removal of the isotropic loading. During the tests, both the longitudinal and shear velocities and the axial and circumferential deformations were measured. 5 and 6 specimens, with different orientation of the schistosity planes, were tested for D- and S-gneiss, respectively.

As an example, in Figure 6 the comparison of the velocities measured in D-gneiss for the specimen $\theta = 0$ ° (only one specimen was loaded under the loading path ID+UN) in ID and UN test is shown. In Figure 7 the comparison of the velocities measured in S-gneiss in two specimens ($\theta = 0$ °, 90 °) in ID and UN test are shown.

Under ID loading conditions a marked increase in velocities is observed with increasing stress. For S-gneiss (Figure 7) the strongest increase in velocities (especially P-wave), with respect to D-gneiss (Figure 6), is recognizable. The anisotropy ratio is progressively reduced for both P- and SR-waves. The velocity trends for specimens with $\theta = 45$ ° (not shown) is quite similar to that observed for the specimens with different schistosity angle. Among the differently oriented specimens the larger gradient of velocities with stress is observed for specimens with schistosity angle equal to 0 °.

Under ID loading conditions the increase of velocities can be related to closure of microcracks perpendicular or oblique with respect to the load axis [4].

In brittle rocks is expected that under uniaxial load conditions the formation of new microcracks, mostly subparallel to the load axis, has a modest influence on the P-wave velocity in the axial direction, and a more significant influence on the S-wave velocity.

In D-gneiss the comparison in the behaviour under uniaxial and isotropic loads was carried out on a single specimen, whose schistosity is perpendicular to the loading axis ($\theta = 0$ °) (Figure 6). The velocity trends of the two tests do not differ substantially, indicating that in this gneiss the new microcracks occur at loads higher than 60 MPa.

Very different is the trend on specimens of S-gneiss. The specimen with schistosity orthogonal to the axis ($\theta = 0$ °) shows that V_P velocities in the UN test (Figure 7), up to 40 MPa, are greater than those detected under isotropic load, probably because during the unloading phase of the ID test not all the microcracks reopened. The phase of opening and forming new microcracks under the deviatoric load is

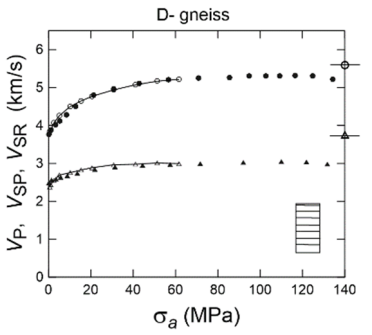

Figure 6. Velocities from ID and UN tests in a specimen with $\theta = 0$ ° of D-gneiss.

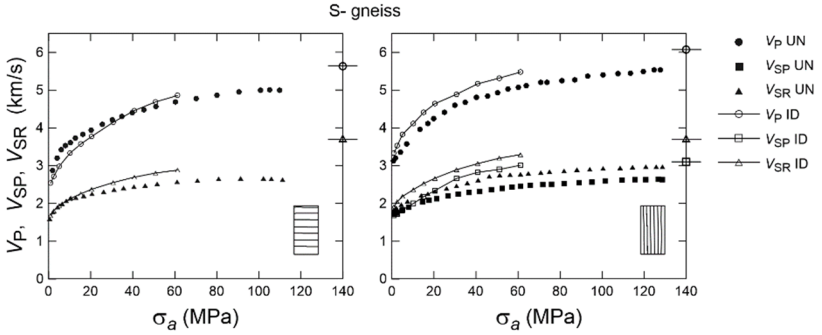

Figure 7. Velocities measured in ID and UN tests in two specimens with $\theta = 0$ ° (left) and $\theta = 90$ ° (right) of S-gneiss. At $\sigma_a = 140$ MPa theoretical intrinsic values for matrix are shown (symbols).

revealed more clearly by the reduced increase of the shear velocities at the load of 10 MPa. In the specimen with schistosity parallel to the axis ($\theta = 90$ °), the velocities already differ from those determined during the ID test at very low loads, presumably as the existing microcracks favourably oriented are mobilized by the deviatoric load.

Regression analyses based on equations (3.6) and (3.7) were carried out for discrete values of the applied stress, providing the global stiffness constants. The trend of the velocities as a function of the schistosity angle θ showed the correspondence between the theoretical model and the experimental values.

On the basis of the average values of the longitudinal and shear velocities, the technical constants (Young's and shear moduli) were calculated, assuming the TI symmetry (par.3.2). All moduli increase with stress. At low pressures, moduli of S-gneiss are lower than D-gneiss, whilst at the maximum pressures the moduli have comparable values, except for modulus E_1 which is higher for D-gneiss.

6.6. Static measurements of deformability

During the uniaxial compression tests with velocity measurement (UN test) (par. 6.5) the axial and circumferential strains were also determined. The measurement was carried out using resistance strain gauges, arranged in pairs, according the scheme in Figure 1.

Uniaxial tests were performed on 11 specimens, with schistosity orientation equal to 0 °, 45 ° and 90 °: 5 and 6 tests were performed on D- and S-gneiss, respectively.

The comparison between specimens with the same orientation, within each pair, shows a fair homogeneous behaviour. All the specimens showed brittle fracture behaviour, more marked in those with schistosity parallel to the loading axis.

At low loads, the axial stress-deformation curves show concavity upwards (to a greater extent in the specimens with $\theta = 0$ °), depending on the progressive closure of favourably oriented microcracks. At higher loads, the dilation for the opening of new cracks prevails over the closure of pre-existing cracks.

From experimental axial and radial strains, the coefficients of the compliance matrix **M,** for discrete values of the applied axial stress, have been obtained applying a regression analysis according to equations (3.3). The statistical analyses were carried out up to a common value of 60 MPa, corresponding to the minimum strength (Table 4). The analyses for the two gneisses were found to be overall satisfactory. The resultant E_1, E_3 and G_{13} engineering moduli are reported in Figure 8 as a function of the axial stress.

Figure 8 evidences a decrease of the Young's moduli at initial loading before the successive rise. The fall is very marked in specimens of D-gneiss at the angle $\theta = 0$ ° (E_3) and S-gneiss at the angle $\theta = 90$ °(E_1). It could possibly be caused by the presence of some closed cracks favourably oriented that begin to slide. Furthermore, at low values of axial stress some cracks could be only potential (for instance crystal boundaries that fail prematurely). Where the increase in moduli is observed, this effect is disguised by the most effective closure of open cracks.

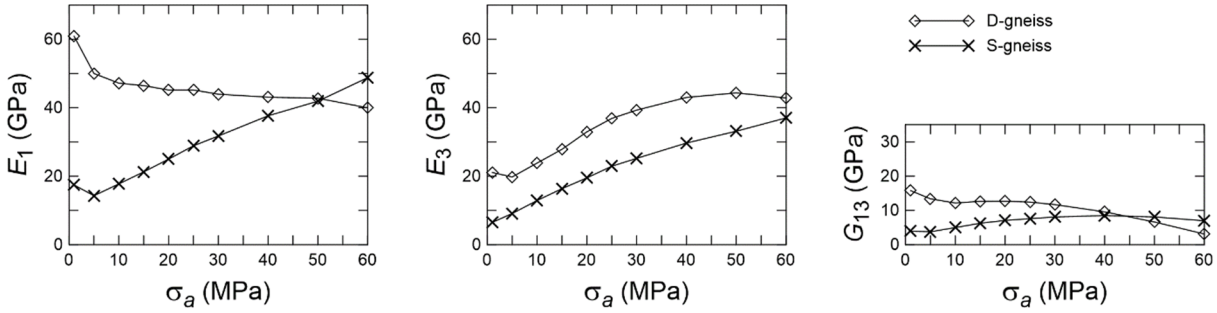

Figure 8. Elastic moduli E_1, E_3 and G_{13} versus axial stress derived by regression analyses for discrete values of the applied axial stress (symbols) for D- and S-gneiss.

A strong difference in the trend of E_1 and G_{13} moduli between the two gneisses is revealed. In S-gneiss the continuous increase of E_1 modulus indicates that the influence of crack closure prevails over the opening of new cracks and that necessarily these cracks are isotropically oriented. In D-gneiss the continuous decrease of E_1 and G_{13} moduli suggests that at low applied stresses, propagation of new cracks and shearing of cracks prevail.

For each value of the axial stress the elastic model provides the global elastic constants of the tested rocks; e.g., the axial deformation gives the apparent Young's modulus E_θ (equation (3.3a)). The trend of the theoretical Young's modulus as a function of the schistosity angle θ for two different axial stress is presented in Figure 9, together with the corresponding experimental values. The Young's moduli of D-gneiss are higher than those of S-gneiss for each value of θ and for all the tested axial stresses (see Figure 8). The anisotropy ratio is reduced as the pressure increases, reflecting the closure of the open microcracks.

At lowest loads, the two transversal deformabilities (ν_{31}/E_3 and ν_{12}/E_1) (equations (3.3b-c)) are independent on specimen orientation and equals, as it is expected in rocks characterized by only one set of open cracks. At higher loads, however, the two deformabilities change as the angle of schistosity varies, as an effect of the shearing of closed cracks. A threshold stress, below which the closure of the microcracks prevails, has been identified for both gneisses at about 30 MPa.

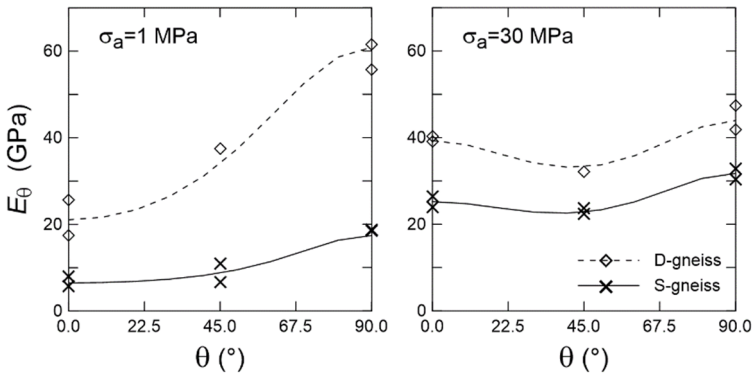

Figure 9. Apparent modulus E_θ versus angle of schistosity measured in single specimens (symbols) and obtained by regression analyses (continuous and dashed lines) for two applied stress, for D- and S-gneiss.

7. Models of deformability

7.1. Synthesis of the dynamic and static deformabilities

In the hypothesis of TI symmetry, the intrinsic parameters of the compliance matrixes $\mathbf{M}_m$ of the two rocks have been calculated (Hill average [13]) assuming the crystal lattices of the phyllosilicate levels (biotite) are iso-oriented, and all the other minerals have not a preferred orientation (Table 5). Such averaging techniques provides quite satisfactory values at high isotropic stress [5]. From the 5 parameters of the TI elastic medium, also the isotropic moduli have been calculated (equation (4.2)) (Table 5).

Table 5. Elastic moduli in case of TI symmetry (left) and isotropy (right) for D- and S-gneiss.

	TI symmetry								Isotropy	
	V_1 km/s	V_3 km/s	V_{13} km/s	V_{12} km/s	E_1 GPa	E_3 GPa	G_{12} GPa	G_{13} GPa	E_m GPa	ν_m
D-gneiss	6.09	5.59	3.05	3.75	91.2	76.8	38.0	25.6	85.84	0.185
S-gneiss	6.07	5.63	3.10	3.72	89.6	77.2	37.2	26.3	85.05	0.196

The different degrees of anisotropy (equation (5.1)) observed in static and dynamic tests under loading account for the closure of open cracks.

Under ID loading conditions, even at the maximum isotropic stress (60 MPa) (Figure 6 and Figure **7**), velocities still increase at significant gradient, indicating that open microcracks are still present. For

the two rocks, even under high compressive stresses, the maximum moduli are lower than those theoretically calculated for the solid matrix (Table 5).

The trend of the anisotropy ratio R_V of the P-waves (average values over the specimens) during loading is shown in Figure 10. In S-gneiss the degree of anisotropy sharply reduces in the initial phase and stabilizes at stresses greater than 10 MPa; conversely in D-gneiss the degree of initial anisotropy is much lower and progressively reduces until a constant value is reached at a stress around 40 MPa.

The behaviour observed in the S-gneiss could derive from closure of very flat (low aperture) microcracks lying within the schistosity plane. D-gneiss, on the other hand, would be characterized by a wider distribution of crack apertures up to higher values, since the pressure necessary to close the microcracks is higher. The final common value around 1.2 is consistent with the anisotropy ratio of the matrix, due to the orientation of crystal lattices (1.19 and 1.16 are the theoretical values for the matrix as TI symmetry is supposed, Table 5).

In UN tests the ratio of anisotropy R_E from the static elastic moduli (equation (5.1)) is influenced by the microcracks forming under loading (Figure 11). As expected, the ratio, initially high, decreases as the load increase, with a sharper gradient for S-gneiss, correspondingly with the dynamic measures. Despite the measured moduli are quite lower than the theoretical values of the solid matrix, due to shearing of closed cracks, at the threshold value of 25-30 MPa the ratio R_E equals the theoretical value (1.19 and 1.16).

The influence of open cracks is also testified by the progressive increase of R_G parameters (equation (5.1)) (Figure 12) with the increase of uniaxial stress for both gneisses. This would comply with the fact that the influence of open cracks diminishes as the applied stress increases, while that of closed cracks increases. This influence happens with a constant rate in D-gneiss suggesting a progressive passage from the closing to the forming of cracks, while in S-gneiss the constant value of R_G in the stress range of 10 - 30 MPa suggests that new cracks possibly appears after 30 MPa.

From UN tests a regression analysis applied at the measured deformabilities according to equation (3.5) provided equivalent moduli of those from equation (3.3), allowing also a direct evaluation of the statistical significance of some parameters. According to the F-test, the second coefficient of regression (estimated value of $1/G_{13}$-$1/G_{SV}$) is significantly (95% probability) different from zero, i.e. the isoG hypothesis cannot be assumed for the tested rock, above the axial stress of 15 MPa and for all the stresses, for D- and S-gneiss, respectively.

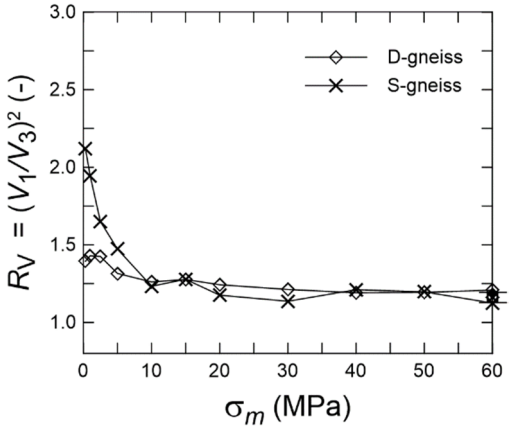

Figure 10. Anisotropy ratio R_V of the P-waves versus mean stress applied during ID tests. The intrinsic values of the matrix are also shown as symbols at 60 MPa.

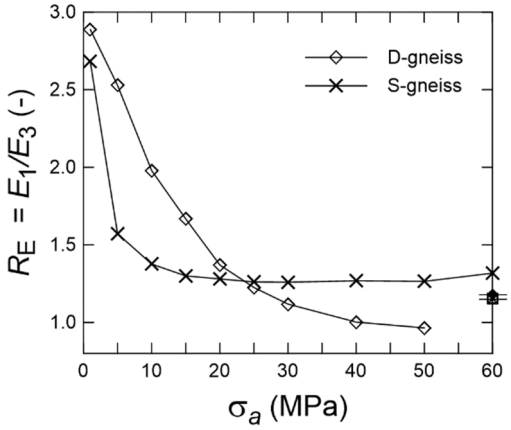

Figure 11. Anisotropy ratio R_E of the Young's elastic moduli versus axial stress applied during UN tests. The intrinsic values of the matrix are also shown as symbols at 60 MPa.

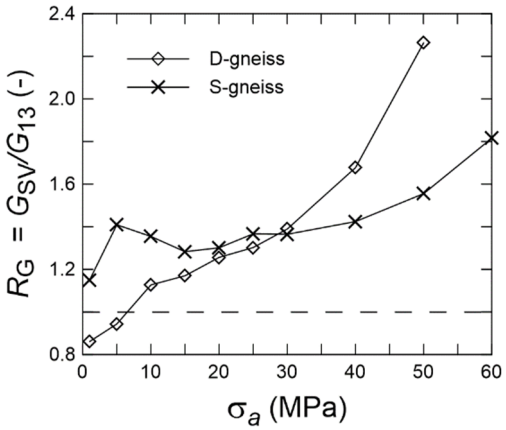

Figure 12. Ratio R_G of the Saint Venant's hypothesis (isoG) versus axial stress applied during UN tests.

The overall behaviour shown in ID and UN tests suggests that two sets of cracks possibly control the rock behaviour. The first set has an orientation corresponding to that of the schistosity plane and consist of cracks very flat that can be closed at low compressive stresses. The second set, which is characterized by randomly oriented cracks with reduced flatness, progressively close under higher stresses.

7.2. Static deformability

In UN test the observed behaviour derives from both open and closed cracks; total deformation sums up that of the uncracked solid plus that of open and closed cracks. Models which account for open and closed cracks predict that closed cracks are considerably less effective than open ones in the reduction of the elastic modulus and that their effect is evident only when specimens have a schistosity angle different from 0 and 90 °. It is thus reasonable to consider the non-linear behaviour observed in UN tests as affected only by open cracks, up to a threshold of the axial stress equal to 30 MPa.

To study the deformability of a cracked medium under loading, an equivalent continuous medium crossed by different sets of open and continuous microcracks was adopted, according the hypothesis explained in par 4.1.

Two sets of microcracks are considered: planar (related to biotite beds) and isotropic (all the other minerals). From the crack frequency counted in crystals of biotite and quartz (Table 1), the mean spacings of cracks were evaluated.

As the examination of the thin sections detected a rhomboid texture of the biotite beds, the planar set is characterized by two cross-planes forming an acute angle of 8 and 12° for D- and S-gneiss, respectively. This texture leads to a non-zero contribution to the transversal deformabilities (ν_{31}/E_3 and ν_{12}/E_1) in specimens loaded normal to the average plane of schistosity.

The isotropic set of cracks is characterized by four cross-planes forming an angle of 45 ° to each other.

The compliance matrix $\mathbf{M}_m$ of the solid matrix has been estimated from equation (4.4) assuming an isotropic intrinsic deformability (Table 5). Thus the compliance matrix of the cracks $\Delta\mathbf{M}_c$ is composed by the contributions of the two sets of cracks: planar $\Delta\mathbf{M}_{c,pl}$ and isotropic $\Delta\mathbf{M}_{c,iso}$:

$$\mathbf{M} = \mathbf{M}_m + \Delta\mathbf{M}_{c,pl} + \Delta\mathbf{M}_{c,iso} \tag{7.1}$$

The compliances of the two sets are due to the normal and shear stiffnesses $(K_n, K_s)_{pl}$ and $(K_n, K_s)_{iso}$, respectively, of the cracks (equation (4.2)), being each formed by two and four equivalent planes.

Comparing the two gneisses, the mean spacing of the planar set of cracks of the D-gneiss is greater than that of the S-gneiss. The same inequality was observed for the spacing of the isotropic set of cracks.

Global deformabilities calculated from UN measures (par. 6.6) allow the estimate of the tangent stiffnesses of the different sets, for discrete values of the applied axial stress up to the threshold of 30 MPa, by applying a regression analysis at equations (7.1). Figure 13 shows the increase of the normal displacement due to cracks $\Delta\delta_n$ (normalized with respect to its maximum) over the axial stress, for both

gneisses. The normalized displacement highlights the relation between the different sets of cracks without depending (as stiffnesses and relative displacements do) on the estimated spacing of cracks, which could have been influenced by the missing counts in other crystals than biotite and quartz.

The discrete integral function of the quantity $\Delta\delta_n$ over the axial stress, that can be easily derived from Figure 13, provides the cumulated closure of the microcracks. For both the gneisses the closure gradient of the cracks of the planar set is higher than the related values of the isotropic set, indicating their quite complete closure at the value of σ_a = 30 MPa. The corresponding isotropic sets of cracks are far to be closed at the stress of 30 MPa. The overall results evidence that in D-gneiss the applied stresses have a reduced capability of closing the microcracks, especially those isotropically distributed, with respect to S-gneiss.

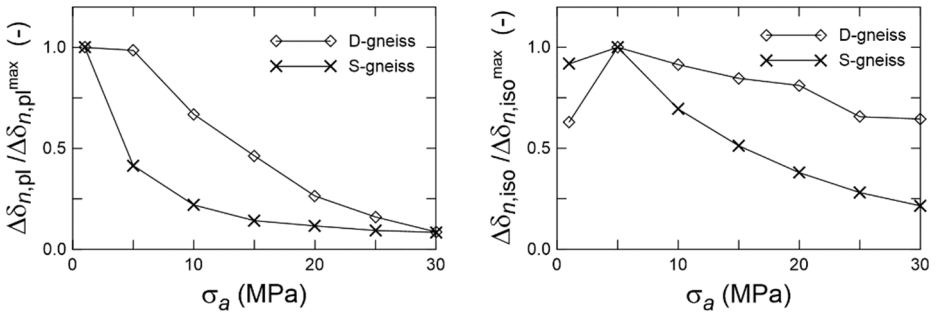

Figure 13. Normalized increase in normal displacement due to cracks (planar set, left; isotropic set, right) versus axial stress in UN tests.

7.3. Dynamic deformability

The effect of cracks on the compliance matrix in the hypothesis of non-interacting cracks were evaluated from the velocity measurements, according to method described in par. 4.2. The components of the crack density tensor have been obtained from the P-wave velocities measured in ID tests in the hypothesis that $F_{11} = F_{22}$.

The intrinsic deformabilities of the gneisses were assumed to have isotropic symmetry, with moduli listed in Table 5.

Assuming that cracks can be modeled as very flat oblate ellipsoids, they will close when the stress normal to the plane of the cracks reaches a critical value σ_{cl} [8] equal to:

$$\sigma_{cl} = \frac{\pi E_m}{4(1-\nu_m^2)}\alpha \tag{7.2}$$

where α is the initial aspect ratio (i.e. opening / diameter ratio) of the cracks.

The variations of the crack density tensors F_{11} and F_{33} have been obtained at different stresses during the tests; then, by means of equation (7.2), they have been related to their aspect ratio.

Assuming a plausible a priori distribution for the orientation of the microcracks allows a more accurate estimate. As already stated, a possible structure for cracks in the investigated gneisses is given by the superimposition of an isotropic set and a planar set of cracks, whose respective densities will be indicated as e_{pl} and e_{iso}. The densities of the two sets are given by:

$$\begin{aligned} e_{pl} &= F_{33} - F_{11} \\ e_{iso} &= 3F_{11} \end{aligned} \tag{7.3}$$

Figure 14 shows the cumulative distribution of the densities of the two sets, as a function of the closure stress or of the aspect ratio, i.e. the global densities of the two sets of cracks which are still open at a given pressure or have an aspect ratio lower than a given value. For both gneisses, aspect ratios of the planar set are markedly lower (below $3\cdot10^{-4}$) than those of the isotropic set. Furthermore, D-gneiss

shows a narrower distribution of aspect ratios of the planar set, consistent with the greater length of microcracks measured in biotite with respect to quartz (Table 1). Thus, for both gneisses, crack-induced anisotropy almost disappears at confining stresses of about 20÷30 MPa.

The higher anisotropy ratio of S-gneiss observed at low stress levels (Figure 10) is coherent with the higher intensity of the crack density e_{pl} compared to e_{iso} isotropic.

As regards the distributions of the isotropic set of crack, the difference between the two gneisses is less relevant, although in D-gneiss the distribution tends to be shifted towards higher aspect ratio values, coherently with the results revealed by the model based on static deformabilities (Figure 13).

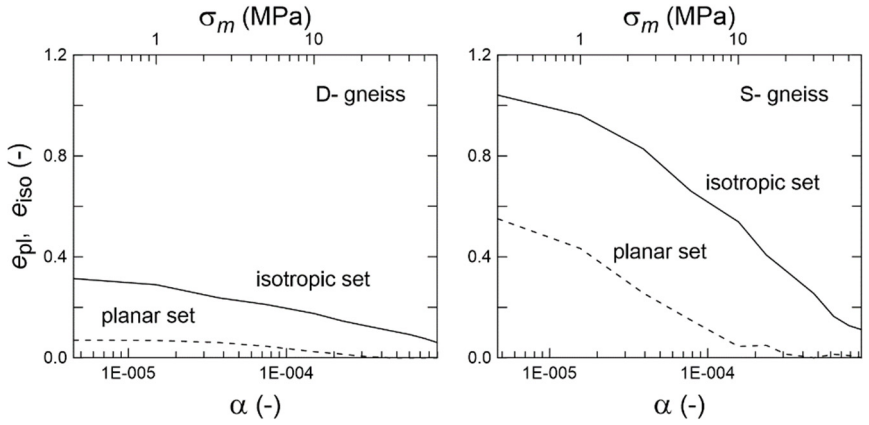

Figure 14. Crack densities of the planar and isotropic sets of cracks deriving from dynamic measures in ID tests versus the applied mean stress (up to 60 MPa) and versus the aspect ratio.

8. Conclusions

In this paper, after a review of simplified theoretical models, some experimental results of an extensive laboratory campaign are presented. Investigations have been conducted over years in the framework of a wider research on anisotropic rocks at both the laboratory and in situ scale ([28] [29]).

The elastic symmetry of rocks derives from the orientation of minerals and microcracks, being the latter factor prevailing at low confining stresses. The ultimate symmetry is due to the superimposition of the various elements of symmetry, and generally, it results of a lower order. The anisotropy of the compliance matrix deriving from minerals (intrinsic matrix) is relevant only at high isotropic stress. In foliated rocks, as microcracking is associated to the cleavage planes of the phyllosilicate crystals, the ultimate symmetry coincides with the intrinsic symmetry.

In this paper the observed deformabilities of two gneisses showing similar strengths and anisotropy ratios in uniaxial compression tests are discussed.

The observed behaviour has been interpreted under the hypothesis that both gneisses are interested by two sets of cracks. The first set has the orientation of the schistosity, with cracks of very low aspect ratios that can be closed at low compressive stresses. Cracks of the second set show a statistically isotropic orientation, have a wider distribution of aspect ratios and close progressively under higher stresses.

Two models which relate the elastic compliance tensor of transverse isotropic materials to the contribution of oriented sets of cracks are presented. It is assumed that the solid matrix has an isotropic behaviour, cracks have equal shape and dimension and crack density is so low that cracks do not interfere each other.

In unstressed conditions measurements of P- and S-wave velocity showed that the gneisses have an orthotropic symmetry, with a very low anisotropy ratio relative to the maximum and intermediate moduli. In the comparison between the gneisses, S-gneiss is characterized by the lower velocities.

The stiffness matrixes of the rocks have been determined from measures of P- and S-wave velocity during triaxial tests under isotropic loading. The fact that for the two rocks (especially for S-gneiss) the maximum measured elastic moduli are lower than those theoretically calculated for the solid matrix by the averaging methods, suggests that the microcracks are not all closed at the maximum pressure of

60 MPa. For both the gneisses, at this pressure the anisotropy ratio of velocities coincides with that of the intrinsic matrix, indicating that no other anisotropy, i.e. iso-oriented cracks, is summed up.

This result is confirmed by the outcomes of the model applied to dynamic measurements. It indicates that in both the gneisses the planar set is characterized by cracks with aspect ratios which close at the pressure of 60 MPa. Conversely, the isotropic set of cracks survives at high pressures and the remaining open cracks have aspect ratios greater than 1E-03.

Strains measured under compressive loading conditions on specimens with different angles of schistosity have provided the elastic compliance matrix. At low uniaxial loads the dependency of axial and transversal deformabilities on the orientation of the specimen is related to the progressive closure of microcracks.

The results from the model applied to static measurements are coherent with those from dynamic measurements, confirming that the isotropic set of cracks is far to be closed at the investigated stresses (especially in D-gneiss). This simple model is capable to differentiate the relative contribute of the two sets of cracks to the deformability and to highlight differences between the tested gneisses.

In this respect, the lower elastic moduli of the S-gneiss in unstressed conditions are due to higher crack densities of both sets, consistently with the values measured on some crystals in thin sections.

It may be inferred that the anisotropy of these rocks under in situ stress is due solely to the cracks, whilst the solid matrix can be considered isotropic.

References

[1] Amadei B 1996 Importance of anisotropy when estimating and measuring in situ stresses in rock *Int. J. Rock Mech. Min. Sci.* **33(3)** 293-325
[2] Auld BA 1990 *Acoustic Fields and Waves in Solids* (Malabar, Florida: Krieger Publ. Company)
[3] Berry P, Crea G, Martino D and Ribacchi R 1974 The influence of fabric on the deformability of anisotropic rocks *Proc. 3rd Int. Congr. Rock Mech*. 105-110
[4] Birch F 1960 The velocity of compressional waves in rocks to 10 kilobars *J. Geophys. Res.* **65(4)** 1083-102
[5] Brace WF 1965 Relation of elastic properties of rocks to fabric *J. Geophys. Res.* **70(22)** 5657-67
[6] Cleary MP, Lee SM and Chen IW 1980 Self-consistent techniques for heterogeneous media *J. Eng. Mech. Div.* **106(5)** 861-87
[7] Condon KJ, Sone H and Wang HF 2020 Low static shear modulus along foliation and its influence on the elastic and strength anisotropy of Poorman schist rocks, Homestake mine, South Dakota *Rock Mech. Rock Eng.* **53(11)** 5257-81
[8] Digby PJ and Murrell SAF 1976 The deformation of flat ellipsoidal cavities under large confining pressures *Bull. Seism. Soc. Am.* **66** 425-431
[9] Ding C, Hu D, Zhou H, Lu J and Lv T 2020 Investigations of P-Wave velocity, mechanical behavior and thermal properties of anisotropic slate *Int. J. Rock Mech. Min. Sci.* **127** 104176
[10] Goodman RE, Taylor RL and Brekke TL 1968 A model for the mechanics of jointed rock *J. Soil Mech. Found. Div.* **94(3)** 637-59
[11] Hakala M, Kuula H and Hudson JA 2007 Estimating the transversely isotropic elastic intact rock properties for in situ stress measurement data reduction: a case study of the Olkiluoto mica gneiss, Finland *Int. J. Rock Mech. Min. Sci.* **44(1)** 14-46
[12] Hearmon RFS 1961 *An Introduction to Applied Anisotropic Elasticity* (Oxford: Oxford University Press)
[13] Hill R 1952 The elastic behaviour of a crystalline aggregate *Proc. Phys. Soc. London* **65** 349-354
[14] Homand FM, Morel E, Henry JP, Cuxac P and Hammade E. 1993 Characterization of the moduli of elasticity of an anisotropic rock using dynamic and static methods *Int. J. Rock Mech. Min. Sci.* **30(5)** 527-535
[15] Horii H and Nemat-Nasser S 1983 Overall moduli of solids with microcracks: load-induced anisotropy *J. Mech. Phys. Solids* **31** 155-171

[16] Hudson JA 1986 A higher order approximation to the wave propagation constants for a cracked solid *Geophys. J. Int.* **87(1)** 265-274
[17] Lekhnitskiĭ SG 1963 *Theory of Elasticity of an Anisotropic Elastic Body* (S. Francisco: Holden-Day, Series in Mathematical Physics)
[18] Kachanov M 1980 Continuum model of medium with cracks *J. Eng. Mech. Div.* **106** 1039-1051
[19] Kachanov M 1992 Effective elastic properties of cracked solids: critical review of some basic concepts *Appl. Mech. Rev.* **45** 304-335
[20] Kim H, Cho JW, Song I and Min KB 2012 Anisotropy of elastic moduli, P-wave velocities, and thermal conductivities of Asan Gneiss, Boryeong Shale, and Yeoncheon Schist in Korea *Eng. Geol.* **147** 68-77
[21] McLaughlin R 1977 A study of the differential scheme for composite materials *Int. J. Engng. Sci.* **15** 237-240
[22] Mori T and Tanaka K 1973 Average stress in matrix and average elastic energy of materials with misfitting inclusions *Acta Metallica* **21** 571-574
[23] O'Connell RJ and Budiansky B 1974 Seismic velocities in dry and saturated cracked solids *J. Geophys. Res.* **79** 5412-5426
[24] Oda M, Suzuki K and Maeshibu T 1984 Elastic compliance for rock-like materials with random cracks *Soils and Foundations* **24** 27-40
[25] Oda M, Yamabe T and Kamemura K 1986 A crack tensor and its relation to wave velocity anisotropy in jointed rock masses *Int. J. Rock Mech. Min. Sci.* **23** 387-397
[26] Ramamurthy T 1993 *Strength and Modulus Responses of Anisotropic Rocks* Comprehensive rock engineering **1(13)** 313-29
[27] Rasolofosaon PN, Rabbel W, Siegesmund S and Vollbrecht A. 2000 Characterization of crack distribution: fabric analysis versus ultrasonic inversion *Geophys. J. Int.* **141(2)** 413-24
[28] Ribacchi R 1988 *Non Linear Behaviour of Anisotropic Rocks* (Berlin, Heidelberg: Springer, Rock and Soil Rheology) 199-243
[29] Ribacchi R, Rotonda T, Totaro L and Zaninetti A. 1999 Evaluation of intrinsic and crack-induced elastic anisotropy in a gneissic rock *9th ISRM Congress*
[30] Salamon MD 1968 Elastic moduli of a stratified rock mass. *Int. J. Rock Mech. Min. Sci.* **5(6)** pp. 519-527
[31] Sayers CM 1988 Inversion of ultrasonic wave velocity measurements to obtain the microcrack orientation distribution function in rocks *Ultrasonics* **26(2)** 73-77

Acknowledgement
The author thanks Liliana Totaro and Holad Mohamed Dahir for having carried out many of the tests. The author thanks Paolo Tommasi for his valuable suggestions.